Journal of Chromatography A 1759 (2025) 466227

Contents lists available at ScienceDirect

Journal of Chromatography A

journal homepage: www.elsevier.com/locate/chroma

Mechanistic modeling of retention time distribution under high breakthrough conditions for continuous Protein A affinity capture

Wu-Wei Chen [a], Yan-Na Sun [a], Yu-Cheng Chen [a], Alois Jungbauer [b], Shan-Jing Yao [a], Hai-Bin Qu [c], Dong-Qiang Lin [a,*]

[a] Key Laboratory of Biomass Chemical Engineering of Ministry of Education, Zhejiang Key Laboratory of Smart Biomaterials, College of Chemical and Biological Engineering, Zhejiang University, Hangzhou 310058, China
[b] Department of Biotechnology, University of Natural Resources and Life Sciences, Vienna, Austria
[c] Pharmaceutical Informatics Institute, College of Pharmaceutical Sciences, Zhejiang University, Hangzhou 310058, China

ARTICLE INFO

Keywords:
Retention time distribution
Residence time distribution
Modeling
Protein A affinity chromatography
Continuous process

ABSTRACT

Regulatory authorities strongly recommend using residence time distribution (RTD) to achieve material traceability in continuous bioprocesses for non-adsorption units. For adsorption-based units, such as chromatography, retention time distribution (ReTD) is more suitable than RTD for characterizing material flow. Continuous capture chromatography is widely applied for biopharmaceutical continuous manufacturing. However, the ReTD behavior in these systems is still not fully understood. In this study, an ReTD model combining general rate model and two-component mobile phase modulator Langmuir model was developed for Protein A affinity chromatography under high breakthrough conditions. The model was calibrated using adsorption equilibrium experiments, protein breakthrough curves and elution curves. It was then validated through pulse injection experiments at varying protein loading phase. The results showed good agreement between model predictions and experimental results ($R^2 > 0.945$). The exchange mechanism between the solid and liquid phases was further analyzed using confocal laser scanning microscopy images and model simulations, revealing that proteins with stronger binding affinity surpass the bound fraction to bind at the adsorption front while those with weaker affinity would exchange with the surface-bound fractions. Finally, simulations of protein distribution in the column during the interconnected loading step indicate that the exchange effect could broaden the ReTD in continuous chromatography. The model developed lays the groundwork for achieving material traceability and enables non-conforming material diversion strategies to facilitate real-time product release in continuous chromatography processes.

1. Introduction

Continuous manufacturing has significant advantages, including consistent product quality, high process efficiency, reduced facility footprint and lower cost [1–5]. Due to intense market competition, the biopharmaceutical industry is progressively transitioning from batch to continuous manufacturing to enhance production efficiency and reduce the cost of goods manufactured (COGM) [6]. To support this shift, ICH has published the Q13 guideline on continuous manufacturing of drug substances and drug products [7], which outlines key principles for establishing continuous integrated manufacturing, with particular emphasis on material traceability. Unlike traditional batch processes, material traceability in continuous processes presents significant challenges due to the complex mass flow dynamics [8]. The Q13 guideline strongly recommends using residence time distribution (RTD) to characterize mass flow and track material throughout the process [7]. The RTD plays a crucial role in process design and control, providing vital information to determine start-up and shut-down times, develop diversion strategies, and define batch sizes [7,9–10]. However, a comprehensive understanding of RTD in continuous bioprocesses remains limited, which hampers the full implementation of continuous manufacturing [11].

Recent studies have reported on the measurement and modeling of RTD in various continuous bioprocess units, including viral inactivation [12–14], virus filtration [15,16], precipitation [17,18] and ultrafiltration [19]. While continuous Protein A affinity chromatography is widely

* Corresponding author at: College of Chemical and Biological Engineering, Zhejiang University, Hangzhou 310058, China.
E-mail address: lindq@zju.edu.cn (D.-Q. Lin).

https://doi.org/10.1016/j.chroma.2025.466227
Received 29 April 2025; Received in revised form 14 July 2025; Accepted 15 July 2025
Available online 16 July 2025

used for monoclonal antibody (mAb) capture, few studies have specifically focused on its RTD behavior [20].

The RTD of protein molecule in chromatography differs significantly from that in other bioprocessing units. Typically, the residence time equals the space time of the fluid flowing through unit volume with a volumetric flowrate. However, due to adsorption behavior in chromatography, the retention time of protein molecule significantly exceeds the space time. Therefore, for such adsorption-based units, a distinct RTD—retention time distribution (ReTD)—should be considered. The differences between ReTD and RTD in bioprocesses are summarized in Table 1.

Continuous Protein A affinity capture has been demonstrated to improve process performance, offering high productivity, efficient resin capacity utilization, and low buffer consumption [21–23]. Several continuous capture modes have been developed [24,25], including CaptureSMB [26], periodic counter-current chromatography (PCC) [27], BioSMB [28] and sequential multi-column chromatography (SMCC) [29]. The interconnected load step is critical for the continuous capture process. In this step, protein is sequentially loaded into two columns interconnected. The first column generally reaches over 70 % breakthrough [21], and the protein breakthrough from the first column can be captured by the second column interconnected. As a result, the protein would distribute into multiple elution peaks during continuous capture, which is different to the single peak in traditional batch capture as shown in Fig. 1. Determining the distribution of specific protein fraction within these peaks is challenging, which certainly complicate material tracking during the continuous capture process. Lali et al. [20] investigated the ReTD in three-column PCC process and tracked the material during the interconnected load step by pulse injection experiments in batch chromatography under high breakthrough conditions, using fluorescently labeled proteins as tracers. The material transferred from the first to second column during the interconnected load step was represented by tracers leaked during the load and wash step. Their results showed that an exchange effect, which is a dynamic process that the protein bound in the solid phase constantly exchanges with the protein in the liquid phase within the resin, complicates mass transfer during the interconnected load step [20]. In the absence of an exchange effect, early-loaded protein would distribute into a single elution peak, as shown in Fig. 1(b). However, when an exchange effect occurs, later-loaded protein would occupy sites initially bound by early-loaded protein, causing the desorbed earlier-loaded protein to migrate from the first to the second column and appear in the second elution peak, as shown in Fig. 1(c). While the tracer experiments have characterized the ReTD in PCC and revealed the exchange phenomenon, mechanistic models are still needed to describe the ReTD behavior and explain the exchange effect in continuous capture processes.

The RTD in chromatography is typically measured using a non-binding tracer [10], which can be used to track the non-interacting molecular during the process. However, in continuous protein A affinity chromatography, material traceability of target product (such as monoclonal antibodies) holds greater significance than that of non-binding small molecules. Since the material traceability of target product cannot be achieved by normal RTD, a distinct RTD of ReTD will be investigated in this study using a labeled protein tracer. The mechanistic chromatography model under high breakthrough conditions will be developed to describe the ReTD behavior and track the target protein for continuous Protein A affinity capture process. The high breakthrough conditions are defined as the loading operation exceeding 70 % breakthrough. The model will be based on the General Rate Model (GRM) and two-component mobile phase modulator Langmuir model, and calibrated by adsorption equilibrium experiments and complete chromatographic curves obtained through off-line measurements. The model will then be validated through tracer experiments using fluorescently labeled proteins as tracer. The developed model can further be used to track the material and explain the exchange phenomenon between liquid-phase and solid-phase antibodies. Finally, the model will be applied to simulate protein distribution within the column during the interconnected load step, investigating the impact of exchange phenomenon on ReTD in continuous capture process.

Table 1
Summary of the differences between ReDT and RTD in bioprocesses.

	Retention time distribution (ReTD)	Residence time distribution (RTD)
Processes characterized	Processes with adsorption (such as chromatography)	Processes without adsorption (such as viral inactivation, ultrafiltration and diafiltration)
Molecule described	Molecules with binding affinity (such as antibodies and FC-fusion protein in chromatography)	Molecules without binding affinity (such as antibodies in diafiltration and salt molecules in chromatography)
Inert tracer	Fluorescently labeled protein	Salt, dextrose and fluorescent dye
Average time spending in unit	Much longer than the space time	Equal to the space time
Models used	Mass transfer equations combined with adsorption and desorption kinetics	Mass transfer equations

2. Theoretical section

The ReTD model was developed with GRM and two-component mobile phase modulator Langmuir model. The GRM and Langmuir models were widely used to describe mass transfer and adsorption behavior in Protein A chromatography [22,23,30,31]. The ReTD analysis also depends on the mass transfer adsorption behavior of a specific material during the process, so these two well-established models were selected to enable the ReTD calculation and characterization in this work. The GRM, which accounts for axial dispersion and film diffusion resistance from the mobile phase to the resin, is given by:

$$\frac{\partial c_i}{\partial t} = -u\frac{\partial c_i}{\partial x} + D_{ax}\frac{\partial^2 c_i}{\partial x^2} - \frac{1-\varepsilon}{\varepsilon}\frac{3}{r_p}k_f\left(c_i - c_{p,i}|_{r=r_p}\right) \tag{1}$$

where c_i (g/L) and $c_{p,i}$ (g/L) represent the protein concentration of mobile phase and intraparticle, respectively. ε (-) is the column porosity. $x \in [0, L]$ (m) and $r \in [0, r_p]$ (μm) are position variables, representing the axial position and the radius of the resin particles. u is the interstitial linear velocity, D_{ax} (m^2/s) is the axial dispersion coefficient and k_f (m/s) is the film mass transfer coefficient. For the components i, $i = 0$ represents the unlabeled component and $i = 1$ represents the tracer component.

The mass transfer within the porous particles, considering both pore and surface diffusion, is given by:

$$\frac{\partial c_{p,i}}{\partial t} + \frac{1-\varepsilon_p}{\varepsilon_p}\frac{\partial q_i}{\partial t} = \frac{1}{r^2}\frac{\partial}{\partial r}\left[r^2\left(D_p\frac{\partial c_{p,i}}{\partial r} + \frac{1-\varepsilon_p}{\varepsilon_p}D_s\frac{\partial q_i}{\partial r}\right)\right] \tag{2}$$

where D_p (m^2/s) and D_s (m^2/s) are the pore and surface diffusion coefficient, respectively. ε_P (-) is the effective particle porosity for protein and q_i (g/L) is the concentration of protein bound in the solid phase. Although mAb exhibits very high affinity adsorption on the Protein A resin and surface diffusion is sometimes ignored [36], the parallel diffusion theory was employed in this work as published in our previous papers [22,23] to more accurately describe protein transport behavior in Protein A affinity chromatography.

To describe the adsorption, two-component mobile phase modulator Langmuir model [40] is used as:

$$\frac{\partial q_i}{\partial t} = k_a e^{\gamma\cdot\left[c(H^+)-c(H^+)_{eq}\right]}c_{p,i}q_{max}\left(1 - \frac{q_0+q_1}{q_{max}}\right) - k_d\left[\frac{c(H^+)}{c(H^+)_{eq}}\right]^{\beta}q_i \tag{3}$$

where k_a (m^3/(mol·s)) and k_d (s^{-1}) are the adsorption and desorption rate

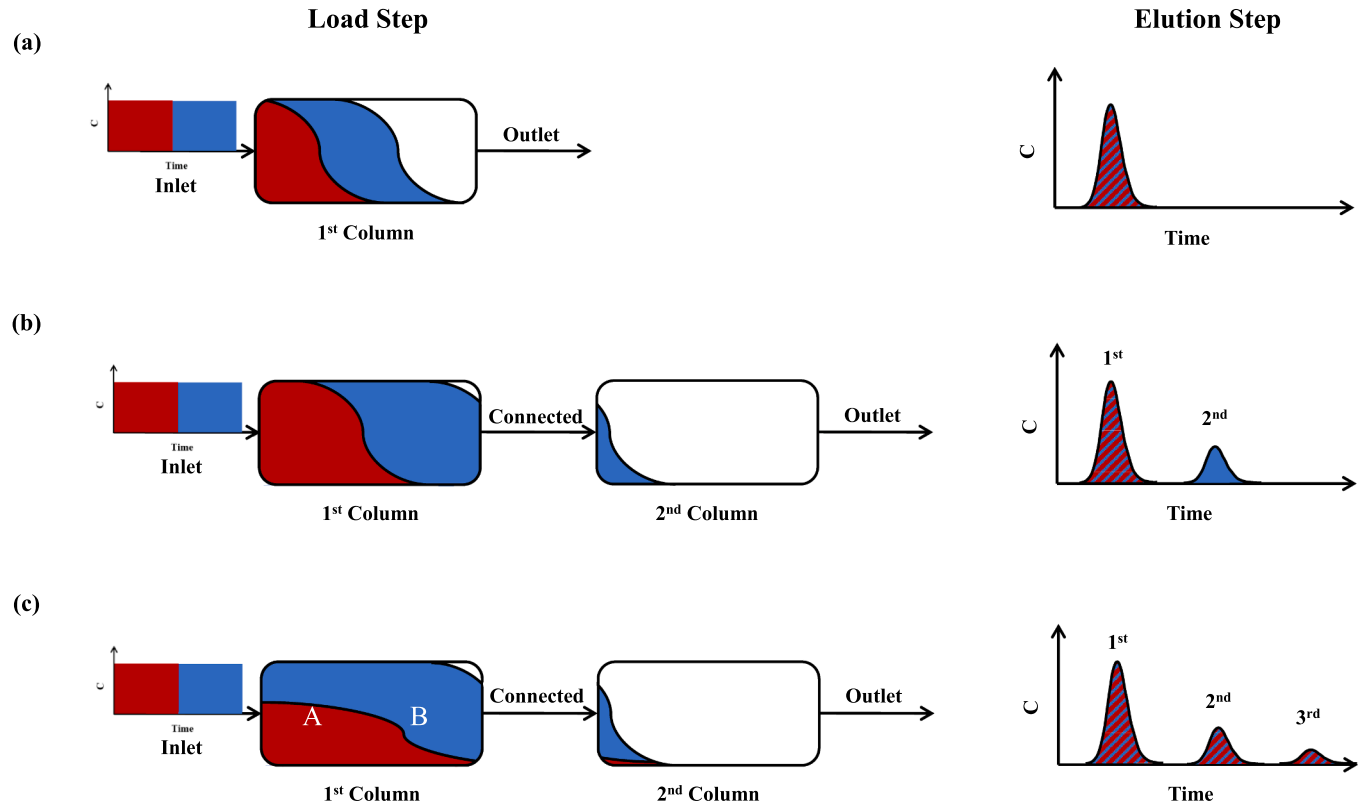

Fig. 1. Scheme of material tracking in Protein A affinity chromatography processes under batch mode (a), continuous mode without exchange effect (b) and continuous mode with exchange effect (c). The red and blue areas represent the protein early-loaded and later-loaded, respectively.

of protein in the equilibration buffer, respectively. $c(H^+)$ (mol/m^3) is the hydrogen ion concentration in the buffer. $c(H^+)_{eq}$ (mol/m^3) is the hydrogen ion concentration in the equilibration buffer. γ (-) and β (-) describes the effect of $c(H^+)$ on the adsorption and desorption rate, respectively. q_{max} (g/L) is the maximum adsorption capacity. Notably, the mass transfer parameters (D_{ax}, k_f, D_p, and D_s) and the adsorption-desorption parameters (k_a, k_d, γ and β) are the same for both the unlabeled and tracer components.

The initial conditions of Eq. (1–3) are set as:

$$c_i|_{t=0} = 0 \tag{4}$$

$$c_{p,i}|_{t=0} = 0 \tag{5}$$

$$q_i|_{t=0} = 0 \tag{6}$$

The boundary conditions at the inlet and the outlet of column are set as:

$$uc_0 - D_{ax}\frac{\partial c_0}{\partial x}|_{x=0} = \begin{cases} uc_{feed}, 0 \le t \le t_a \\ 0, t_a \le t \le t_b \\ uc_{feed}, t_b \le t \le t_c \\ 0, t_c \le t \le t_e \end{cases} \tag{7}$$

$$uc_1 - D_{ax}\frac{\partial c_1}{\partial x}|_{x=0} = \begin{cases} 0, 0 \le t \le t_a \\ uc_{feed}, t_a \le t \le t_b \\ 0, t_b \le t \le t_e \end{cases} \tag{8}$$

$$uc(H^+) - D_{ax}\frac{\partial c(H^+)}{\partial x}|_{x=0} = \begin{cases} c(H^+)_{eq}, 0 \le t \le t_d \\ c(H^+)_{elution}, t_d \le t \le t_e \end{cases} \tag{9}$$

$$\frac{\partial c_i}{\partial x}|_{x=L} = 0 \tag{10}$$

where c_{feed} (g/L) is the protein concentration in the feedstock, and $c(H^+)_{elution}$ (mol/m^3) is the hydrogen ion concentration in the elution buffer. t_a (s), t_b (s), t_c (s), t_d (s) and t_e (s) represent the start of the tracer injection, the end of the tracer injection, the end of the load step, the end of the wash step and the end of the elution step, respectively. During the entire load step $t \in [0, t_c]$, the feeding is continuous, with the protein and tracer fed into the column alternately.

The boundary conditions at the center and the surface of the resin particle are set as:

$$\frac{\partial c_{p,i}}{\partial r}|_{r=0} = 0 \tag{11}$$

$$D_p\frac{\partial c_{p,i}}{\partial r}|_{r=r_p} + \frac{1-\varepsilon_p}{\varepsilon_p}D_s\frac{\partial q_i}{\partial r}|_{r=r_p} = \frac{1}{\varepsilon_p}k_f\left(c_i - c_{p,i}|_{r=r_p}\right) \tag{12}$$

3. Materials and methods

3.1. Materials

MabSelect SuRe LX resin was purchased from Cytiva (Uppsala, Sweden). The resin was packed into a Tricon 5/50 column (0.5 cm diameter) from Cytiva (Uppsala, Sweden) to a bed height of 5.0 cm. The IgG1-type mAb and the FC-fusion protein (FC-protein) were provided by a local biological company and used as model proteins. The Alexa Fluor 488 fluorescent labeling kit was purchased from Invitrogen (CA, USA). All other chemicals were of analytical reagent grade.

3.2. Fluorescent labeling

Alexa Fluor 488 fluorescent dye was used to label both the mAb and FC-protein according to the manufacturer's guidelines. The labeled fluorescently protein was purified using Pierce centrifuge columns

(Thermo Scientific, MA, USA) and 10 kDa membrane filters (Merck Millipore, MA, USA). To ensure complete removal of the free dye, the filtration step was repeated until the fluorescence intensity of the filtrate measured by Spectra max M5 multi-mode microplate readers (Molecular Device, CA, USA) was below the detection limit. The excitation and emission wavelength of the fluorescence detector were set to 490 nm and 525 nm, respectively. The degree of labeling (DOL) was assessed following the manufacturer's guidelines. To ensure that the protein structure remained intact, the DOL was maintained consistently below 1 [20].

3.3. Adsorption equilibrium experiment

The adsorption isotherms of mAb and FC-protein on MabSelect SuRe LX resins were determined by batch experiments. Protein stock solutions were initially prepared at 10 g/L in equilibration buffer (50 mM phosphate, 500 mM NaCl, pH 7.4) and then diluted to specific concentrations with equilibration buffer. The resin beads were pre-equilibrated with equilibration buffer and then drained. Then 0.03 g drained resin was mixed with 0.8 mL protein solution at different concentrations (0.5~10 mg/mL), and incubated on a thermomixer (Thermo Scientific, MA, USA) at 1200 rpm and 25 °C for 5 hours. After adsorption equilibrium was reached, the protein concentration of the supernatant was measured by Unano-1000 micro-spectrophotometer (Yomim, China). The amount of absorbed protein at equilibrium was calculated by a mass balance. The adsorption isotherms were fitted to the Langmuir isotherm equation, given by

$$Q = \frac{Q_{max} C}{K_d + C} \tag{13}$$

where Q and C represent the equilibrium adsorption capacity of the resin (mg/g resin) and the equilibrium protein concentration in the liquid phase (g/L), respectively. Q_{max} is the maximum adsorption capacity of the resin (mg/g resin) and K_d is the desorption equilibrium coefficient (g/L).

3.4. Batch chromatography experiment under high breakthrough percentage

Batch chromatography experiments were performed using an ÄKTA Pure chromatography system (Cytiva, Uppsala, Sweden) with feed concentrations of 1, 2, and 6 g/L for mAb, and 1, 2, and 4 g/L for FC-protein. The feedstocks were prepared using equilibration buffer (50 mM phosphate buffer, 500 mM NaCl, pH 7.4). The proteins were loaded until a 70 % breakthrough percentage was reached, followed by a 5 CV wash with equilibration buffer and a 6 CV elution with 150 mM sodium buffer (500 mM NaCl, pH 3.2). The flow rate for all steps was 0.5 mL/min. The outlet of all steps was collected in 0.5 mL fractions and analyzed using a Unano-1000 detector to measure the protein concentration.

3.5. Pulse injection experiments

The pulse injection experiments with labeled protein to measure the ReTD was conducted by an ÄKTA Pure chromatography system. The details of the experiments are provided in Table 2. 500 mM NaCl was added in the equilibration, loading and washing buffers to minimize the differences in retention time between labeled and unlabeled proteins [20]. To characterize the ReTD behavior at different loading time, the labeled protein was injected through a 500 μL sample loop at start (Phase I), middle (Phase II) and end (Phase III) of the loading step, as shown in Fig. 2. In particular, injections were performed at the breakthrough percentages of 0 %, 35 %, and 65 %. The fractions during the loading, injection, washing and elution steps were collected and analyze for the labeled protein concentration using a Spectra Max M5 multi-mode microplate reader. The excitation and emission wavelength of the fluorescence detector were set as 490 nm and 525 nm, respectively.

Table 2
Parameters of pulse injection experiments.

Steps	Amount	Solution	Flow rate (mL/min)	Collection
Equilibration	5.0 CV	50 mM phosphate buffer, 500 mM NaCl, pH 7.4	0.5	No
Load	Until 70 % breakthrough percentage	2 g/L protein	0.5	Yes
Injection*	0.5 CV	2 g/L fluorescently labeled protein	0.5	Yes
Wash	5.0 CV	50 mM phosphate buffer, 500 mM NaCl, pH 7.4	0.5	Yes
Elution	5.0 CV	150 mM citrate buffer, 500 mM NaCl, pH 3.2	0.5	Yes

* The labeled protein was injected at breakthrough percentage of 0 %, 35 % and 65 %.

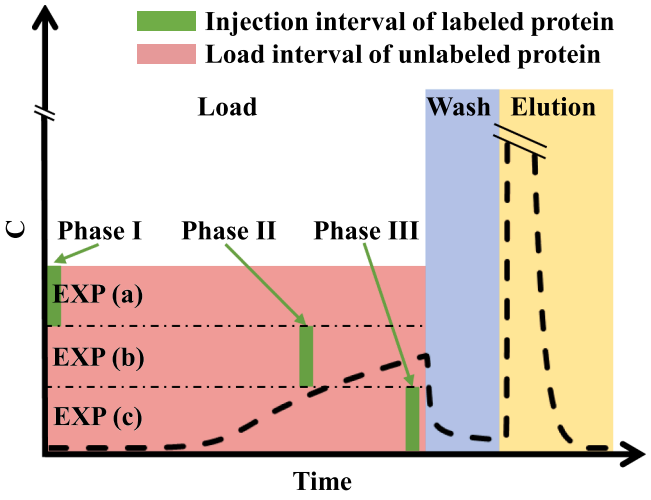

Fig. 2. Experimental scheme of pulse injection at start (Phase I), middle (Phase II) and end (Phase III) of the loading step.

3.6. Process simulation

The chromatography analysis and design toolkit (CADET) was used for chromatographic process simulation. CADET provides numerical tools for solving the partial differential equations of chromatographic models [32,33]. GRM was used as column model and two-component mobile phase modulator Langmuir model was used as binding model. The operation parameters were listed in Table 2 and the determined model parameters were listed in Table 3. The number of finite elements along both the x-axis and r-axis in GRM was set to 100, and the time step size was set to less than 0.1 s.

3.7. Model calibration

Based on the theoretical framework described in Theoretical Section, the model parameters (r_p, D_{ax}, k_f, ε, ε_p, D_p, D_s, k_a, k_d and q_{max}) need to be determined. The r_p of MabSelect SuRe LX resin is 42.5 μm, as provided by the manufacturer. ε and ε_p were measured by the pulse injection experiments under non-binding conditions with blue dextran and model

Table 3
Model parameters for mAb and FC-protein.

Model parameters	mAb	FC-protein
r_p (μm)	42.5	
L (m)	0.05	
D_{ax} (10^{-6} m^2/s)	3.57	3.75
k_f (10^{-5} m/s)	1.38	1.48
ε (-)	0.42	0.40
ε_p (-)	0.64	0.59
D_p (10^{-12} m^2/s)	5.68	1.62
D_s (10^{-15} m^2/s)	2.34	1.37
k_a (m^3/(mol·s))	9.12	9.61
K_d (10^{-3} g/L)	4.83	12.2
q_{max} (g/L resin)	129.3	76.9
β (-)	0.93	0.95
γ (-)	−1.87	−1.52

proteins as tracers [33]. D_{ax} was estimated from the hydrodynamic dispersion using the relation $D_{ax} = uk_{ed}$, where $k_{ed} = 0.09$ cm [34]. k_f was estimated using the correlation by Wilson and Geankoplis [35] as

$$k_f = \frac{D_m}{2r_p}\frac{1.09}{\varepsilon}\left(\frac{2ur_p}{D_m}\right)^{\frac{1}{3}} \tag{14}$$

where D_m is the free diffusion coefficient, typically 1.66 cm^2/s for mAb [11]. K_d can be determined by static binding experiments, as described by Eq. (13). k_d is expressed as $K_d \times k_a$. The parameters D_p, D_s, k_a, and q_{max} were determined for the breakthrough curves using the inverse method. The inverse method can be regarded as an optimization problem, given by Eq. (15).

$$\min_{D_p,D_s,k_a,q_{max}} \left[f\left(D_p, D_s, k_a, q_{max}\right)\right] \tag{15}$$

The objective function in Eq. (15) is given by

$$f\left(D_p, D_s, k_a, q_{max}\right) = \sum_{i=1}^{k} \frac{1}{\| c_i^{EXP} \|_{L^2}^2} \| c_i^{EXP} - c_i^{CAL}\left(t, c_{feed}; D_p, D_s, k_a, q_{max}\right) \|_{L^2}^2 \tag{16}$$

where c_i^{EXP} and c_i^{CAL} represent the experimental and calculated protein concentrations, respectively. Similarly, parameters γ and β can be determined by elution profiles, given by Eq. (17).

$$\min_{\gamma,\beta}\left[\sum_{i=1}^{k} \frac{1}{\| c_i^{EXP} \|_{L^2}^2} \| c_i^{EXP} - c_i^{CAL}(t;\gamma,\beta) \|_{L^2}^2\right] \tag{17}$$

The optimization problem was solved using a genetic algorithm (GA). The maximum iterations were set to 200 [33]. The population size and the mutation probability were determined by the grid search optimization as shown in Fig. S1 (Supporting information). The results revealed that the model output became insensitive to the parameter variations when the population size exceeded 100 and mutation probability fell below 0.002. After evaluation of both computational efficiency and optimization effectiveness, the population size of 100 and the mutation probability of 0.001 was selected in the inverse method.

3.8. ReTD characterization

The concentration profiles of the labeled protein at the outlet of column ($c_1(t)$) represent the ReTD behavior in Protein A chromatography, which can either be simulated by the model or measured in impulse injection experiments. The simulated cumulative ReTD $F(t)$ can be expressed as:

$$F(t) = \frac{\int_0^t c(t)dt}{(t_b - t_a)c_{feed}} \tag{18}$$

where $F(t)$ represents the percentage of the tracer that has exited the column from 0 to t, relative to the total amount injected. Assuming that all the protein has left the column by the end of the elution step, the experimental $F(t)$ can be calculated as:

$$F(t) = \frac{\int_0^t c(t)dt}{\int_0^{t_e} c(t)dt} \tag{19}$$

where t_e denotes the end time of the elution step. The percentage of the tracer leaked during the loading and washing step (P_{lw}) is used to characterize the ReTD behavior in Protein A chromatography. P_{lw} can be calculated as:

$$P_{lw} = \frac{\text{amount of tracer leaked in load and wash step}}{\text{amount of tracer}} = F(t_d) \tag{20}$$

4. Results and discussion

4.1. ReTD model calibration

The ReTD model was calibrated through four steps. Firstly, D_{ax} and k_f were determined using the empirical formulas, while ε and ε_p were measured by the pulse injection experiments under non-binding conditions with blue dextran and model proteins as tracers. Secondly, K_d was fitted with the adsorption equilibrium experiments. Fig. 3 shows the adsorption isotherms for mAb and FC-protein, along with the correlation results using Eq. (13). Thirdly, D_p, D_s, k_a and q_{max} were fitted with the protein breakthrough curves with various feed concentrations. Guo et al. [36] found that the binding affinity of the protein to the resin primarily influences the shape of the wash profile, while the mass transfer rate mainly affects the shape of the load profile. To accurately estimate the adsorption and mass transfer parameters, both the load and wash profile from the breakthrough experiments were used to calibrate the model. Fig. 4 compare the calculated results with the experimental data for mAb and FC-protein breakthrough experiments. The R^2 values were 0.982 for mAb and 0.989 for FC-protein, indicating a strong agreement between the simulated results and experimental data. Finally, the parameters β and γ were fitted by the elution curves as shown in Fig. 5. The final model parameters obtained are summarized in Table 3.

4.2. ReTD behavior in Protein A affinity chromatography

The pulse injection experiments were conducted using the fluorescently labeled protein as inert tracer to investigate the ReTD behavior in Protein A affinity chromatography. Fig. 6 show the results of pulse injection experiments at the start (Phase I), middle (Phase II) and end (Phase III) of the loading step for mAb. The concentration of labeled protein was detected in the loading, washing and elution steps after the labeled protein injection. The labeled protein concentration profiles represent ReTD profiles corresponding to different injection times. The ReTD profiles differ from the RTD observed in non-adsorption units such as tubular reactors. Normal RTD behavior typically exhibits a single peak in its distribution profile. However, due to the adsorption-desorption effects of Protein A affinity chromatography, the ReTD behavior showed a bimodal distribution with two distinct peaks. Moreover, while materials entering at different time would normally display identical RTD behavior in non-adsorption units, the ReTD behavior in affinity chromatography system varies with time. Specifically, when the injection occurred at Phase I, the ReTD profile gradually increased during the loading step (Fig. 6(a3)). When the injection was at Phase II, the labeled protein quickly exited the column after injection, followed by a sustained leakage (Fig. 6(b3)). When the injection was at Phase III, only a tailing peak could be observed in the loading step (Fig. 6 (c3)). Similar ReTD profiles were also observed in the pulse injection experiments for FC-protein, as shown in Fig. 7, with more significant sustained leakage in both Phase I and Phase II. Lali et al. [20] also observed the leakage phenomenon, attributing it to the constant

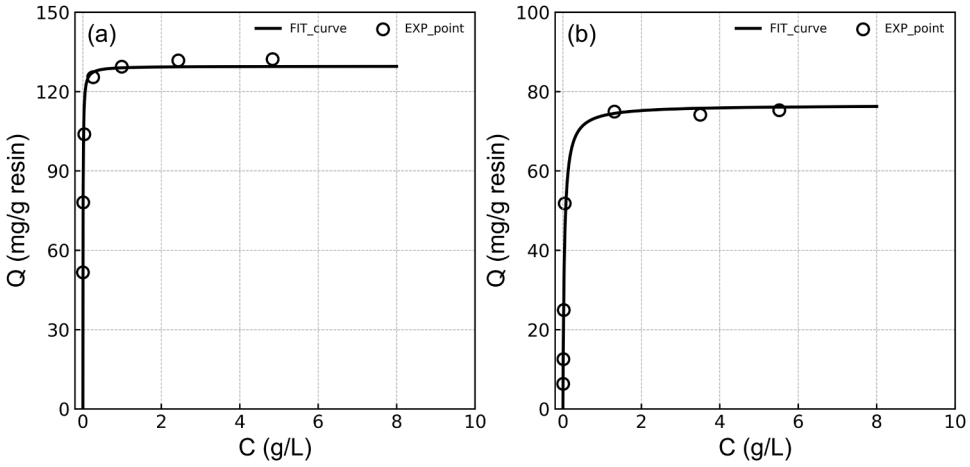

Fig. 3. Model fitting for adsorption isotherms of mAb (a) and FC-protein (b).

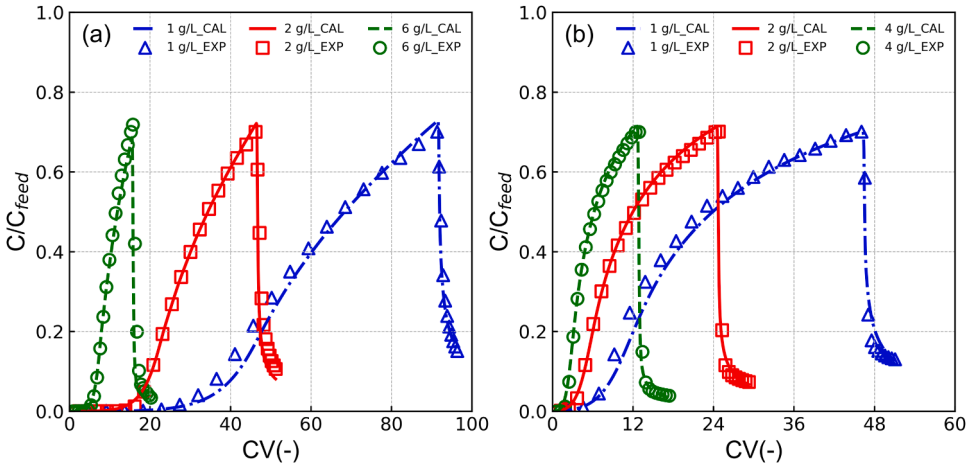

Fig. 4. Comparison of the calculated breakthrough curves with the experimental data of mAb (a) and FC-protein (b) at varying feed concentration.

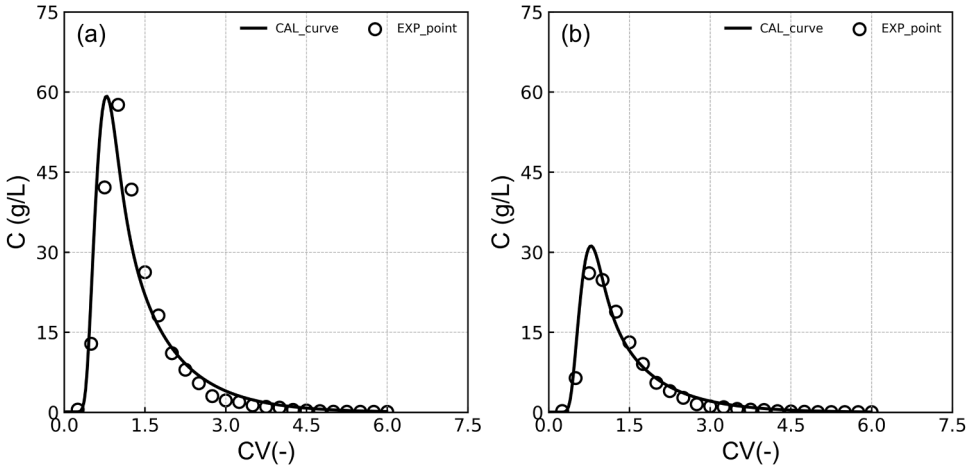

Fig. 5. Comparison of the calculated elution curve with the experimental data of mAb (a) and FC-protein (b).

exchange between the antibody in the liquid phase and the solid phase. Specifically, when the tracer was injected at Phase I, none of the labeled protein exited the column immediately because sufficient binding sites were available. The bound protein gradually desorbed and exited the column during the feeding, resulting in sustained leakage. When the labeled protein was injected at Phase II, the adsorption rate was slower than the mass transfer rate under overload conditions [37], causing some of the labeled protein to exit the column immediately. As feeding continued, the bound labeled protein in the solid phase constantly exchanged with the protein in the mobile phase and gradually leave the column.

To further quantify the exchange effect, $F(t)$ and the percentage of tracer leaked during the load and wash step (P_{lw}) was calculated. When the labeled protein was injected at the breakthrough percentages of 0 %,

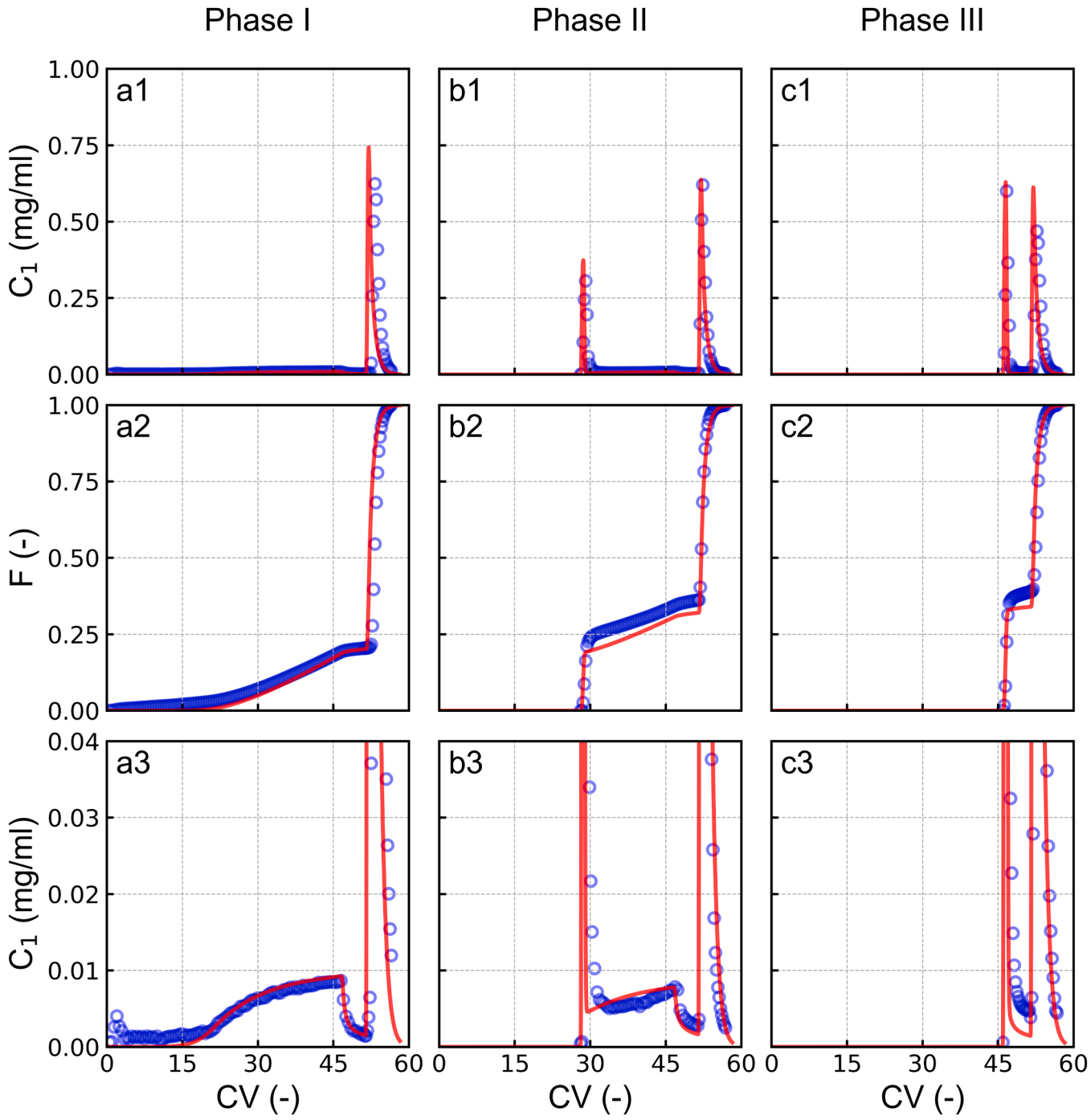

Fig. 6. Pulse injection experiments of mAb at start (Phase I) (a), middle (Phase II) (b) and end (Phase III) (c) in the load step with MabSelect SuRe LX resin. Rows 1 to 3 show the labeled protein concentration at the outlet, *F*-curves and the magnified view of the tracer concentration at the outlet, respectively. The blue circles are the experimental data and the red lines show the model predicted results.

35 % and 65 %, the P_{lw} values were 21.9 ± 1.6 %, 36.5 ± 0.8 % and 38.3 ± 0.5 % for mAb and 37.1 ± 1.2 %, 44.2 ± 1.7 % and 38.9 ± 0.6 % for FC-protein, respectively. In the absence of exchange, the P_{lw} values should theoretically equal the injection breakthrough percentage [20]. The observed discrepancies between the P_{lw} values and the injection breakthrough percentage indicated that significant exchange occurs in the Protein A affinity chromatography.

In brief, the exchange phenomenon can be confirmed through the ReTD profiles and the P_{lw} values. Desorption is less noticeable in conventional batch chromatography [20], as the desorbed protein is re-adsorbed onto the unused binding sites further in the column. In contrast, in the continuous chromatography, the resin is nearly fully loaded and the desorbed protein would move to the next column, making desorption more significant. Therefore, both adsorption and desorption must be incorporated into the ReTD modeling of continuous capture process to accurately describe the exchange phenomenon.

4.3. *ReTD model validation*

The calibrated ReTD model was used to predict the ReTD profiles observed in the pulse injection experiments. The pulse injection experiments settings are listed in Tabel 1. Figs. 6 and 7 show the comparison

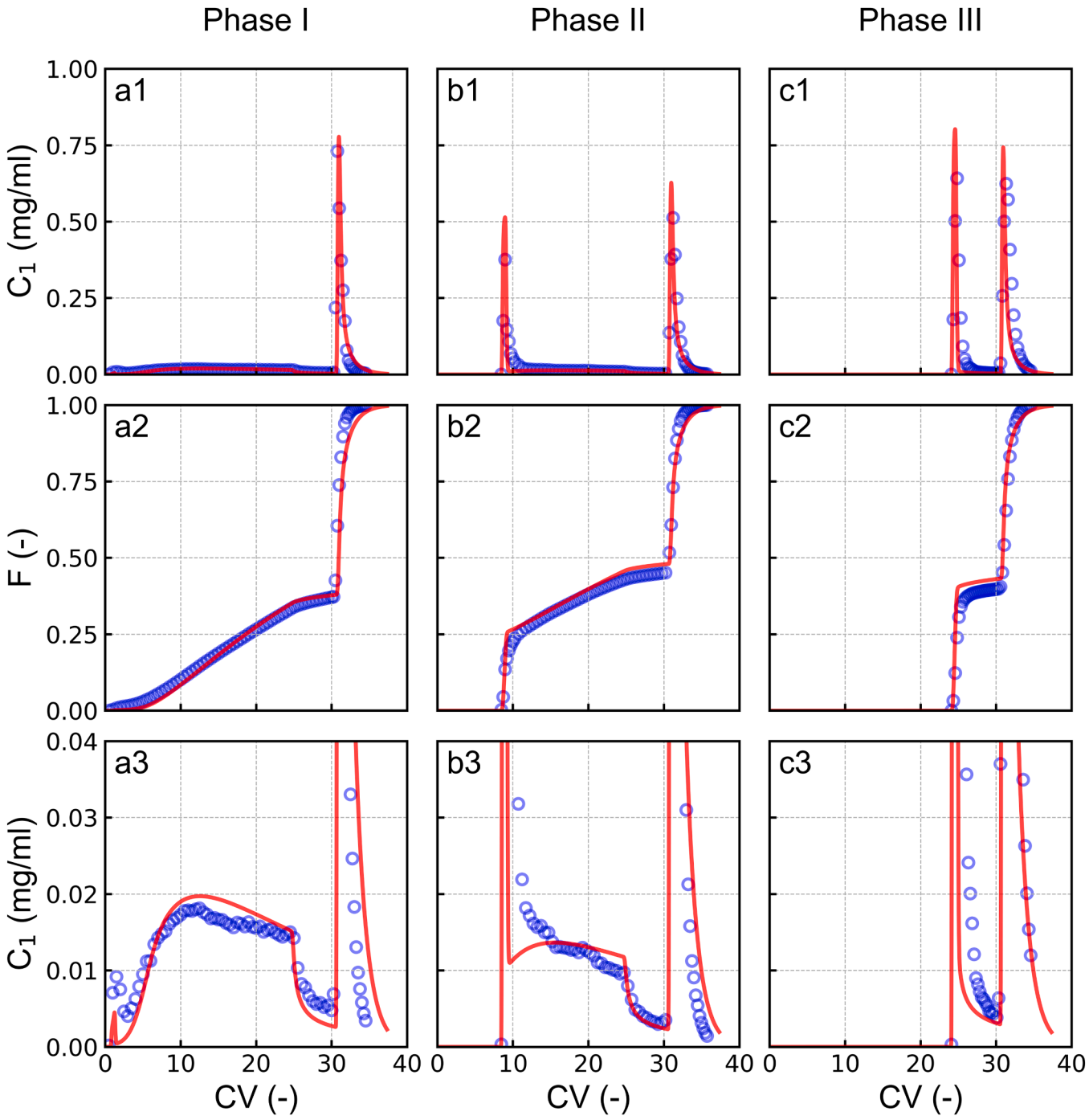

Fig. 7. Pulse injection experiments of FC-protein at start (Phase I) (a), middle (Phase II) (b) and end (Phase III) (c) in the load step with MabSelect SuRe LX resin. Rows 1 to 3 show the labeled protein concentration at the outlet, *F*-curves and the magnified view of the tracer concentration at the outlet, respectively. The blue circles are the experimental data and the red lines show the model predicted results.

between the model predicted and experimental results for mAb and FC-protein, respectively. The predicted ReTD profiles match the experimental profiles well with R^2 values of 0.962 and 0.945 for mAb and FC-protein, respectively. The slight differences between the calculated and experimental data may be attributed to the presence of residual free dyes in the labeled protein solution and the diffusion effects from peripheral equipment. To evaluate the model performance in the calibration and validation datasets, the mean error (ME) and root mean square error (RMSE) of normalized protein concentration for the datasets were calculated, and the results are listed in Table S1 (Supporting information). It was found that the ME values for all datasets were close to zero, and the RMSE values of the validation datasets were comparable to those of the calibration datasets. To further evident the consistent performance in both calibration and validation sets, the Kolmogorov-Smirnov (K-S) test for the residuals distributions of the datasets were implemented. It was found that the residuals distributions between calibration and validation datasets were similar as shown in Figs. S2 and S3 (Supporting information). The K-S test revealed no statistically significant difference at $\alpha = 0.01$ ($p = 0.024$ and 0.063 for FC-protein and mAb, respectively), supporting the assumption of identical underlying distributions. Based on above results, it could be concluded that the developed model has a good and consistent performance on both

calibration and validation datasets and the risk of overfitting is minimal. Notably, the model could accurately describe the exchange phenomenon, including the sustained leakage in Phases I and II and the tailing peak in Phase III. This predictive capability is enabled by the model's incorporation of both mass transfer and adsorption-desorption kinetics. Furthermore, the labeled and unlabeled proteins are treated as two components with identical mass transfer and adsorption-desorption rates in the model. This approach is crucial for accurately predicting the ReTD profiles. Such parameterization aligns with the fundamental principle of time distribution characterization, which requires that the tracer component behaves identically to the normal component [38]. Although this approach has been widely used in RTD analysis for various unit operations [10], to our knowledge, this is the first application in ReTD modeling for Protein A chromatography.

More significant sustained leakage was observed in Phase I and II for FC-protein than for mAb in the pulse injection experiments. This might be attributed to the lower binding affinity of FC-protein toward Protein A resin compared to mAb (Fig. 3), which would result in more exchange and leakage. In the model, the parameter K_d could quantitatively represent the exchange strength, allowing for an accurate prediction of the distinct ReTD behaviors of the two proteins in Protein A chromatography.

In summary, the model can effectively characterize the exchange phenomenon by incorporating both mass transfer and adsorption-desorption kinetics, and it can reliably predict the ReTD behavior under varying breakthrough percentage of injection. This provides a solid foundation for further analysis of the mechanism behind the exchange phenomenon.

4.4. Mechanistic analysis on the exchange phenomenon

To elucidate the underlying mechanism on the exchange phenomenon, the developed ReTD model was employed for CLSM imaging simulation through in-silico step-wise injection experiments. Specifically, the resin beads were sequentially loaded with unlabeled protein (Stage I), followed by labeled protein (Stage II), and then unlabeled protein again (Stage III), as shown in Fig. 8. In each stage, the amount of loaded protein was equal to 40 % of the binding capacity. The concentration profiles of both labeled and unlabeled protein during the three stages were calculated, focusing on the 50th element along the x-axis, which was located in the middle of the column.

Fig. 8 shows the CLSM simulation results of FC-protein. In Stage I, unlabeled protein was loaded into the column. In Stage II, the labeled protein bound to the surface of the resin. In Stage III, the subsequently loaded unlabeled proteins occupied the surface layer above the pre-adsorbed labeled proteins, while the labeled fraction gradually migrated from the surface towards the center of the resin. According to the simulation results, the binding sites on the resin surface were fully saturated in Stage I. During the loading of labeled protein in Stage II, the surface concentration of the labeled protein ($q_1|_{r=r_p}$) gradually increased, while the concentration of the unlabeled protein ($q_0|_{r=r_p}$) decreased, with the total surface protein concentration ($q_0|_{r=r_p} + q_1|_{r=r_p}$) remaining constant at 1.5 mol/m^3. If there is no exchange, the concentration of the unlabeled protein should be constant as 1.5 mol/m^3 in Stage II. The model's description of surface concentration profiles demonstrated its capacity to characterize the protein exchange mechanism at the resin surface.

Additionally, CLSM simulations of mAb were performed as shown in Fig. 9. The results revealed significant differences between mAb and FC-protein. Firstly, mAb exhibited a sharper adsorption front than FC-protein as shown in the total protein concentration profiles (Figs. 8(b) and 9(b)). This front is consistent with a fast pore diffusion mechanism according to the shrinking core theory [39]. Due to the lower transfer resistance of mAb, the desorbed mAb would penetrates deeper into the resin compared to FC-protein (Fig. 8(b6) and 9(b6)). Secondly, when the binding sites on the resin surface were fully saturated, mAb predominantly bound to the inner of the resin at the adsorption front (Fig. 8(a4) and (b4)), whereas FC-protein primarily adsorbed onto the surface (Fig. 9(a4) and (b4)). The stronger binding affinity of mAb would reduce the exchange effect, allowing more mAb to surpass the bound fraction and bind at the adsorption front. Overall, the lower desorption rate and faster pore diffusion would enable the mAb to penetrate more deeply into the resin, while the FC-protein mainly migrates out of the resin through liquid-solid exchange on the surface. The simulation results also explain the distinct ReTD behaviors observed for mAb and FC-protein in the pulse injection experiments. Due to its less desorption and deeper

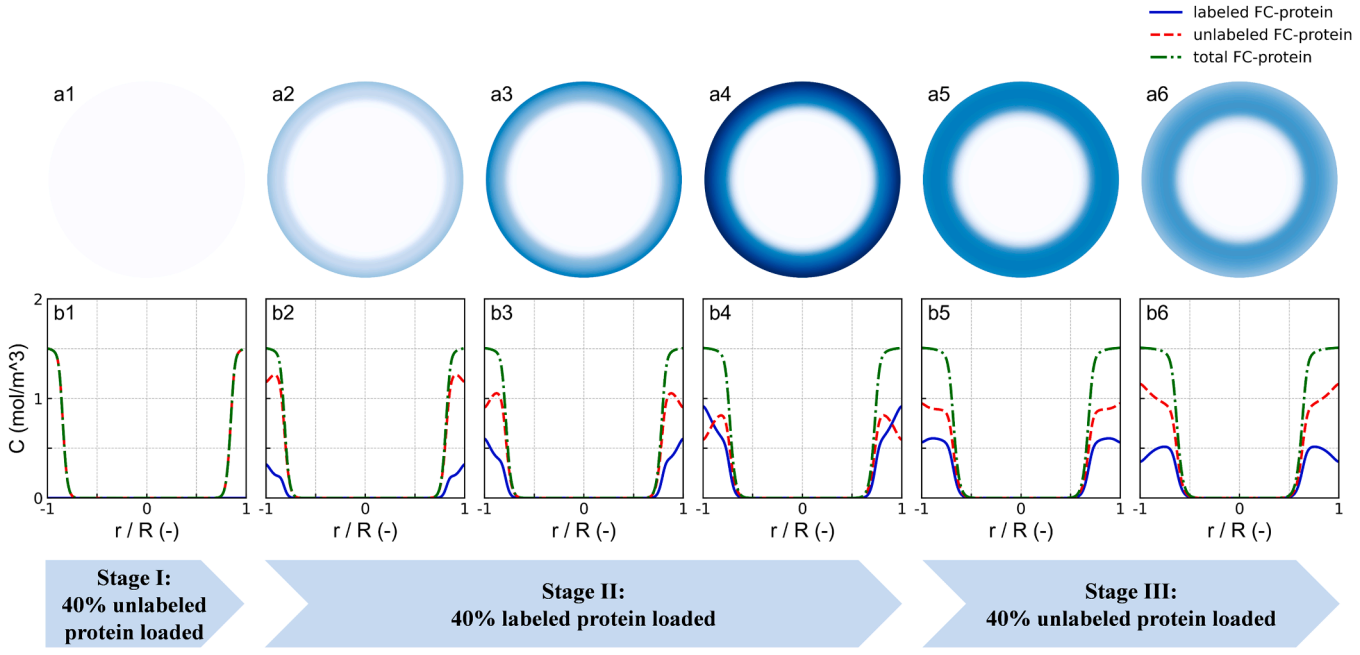

Fig. 8. Simulation results of CLSM for FC-protein during three load stages. (a) The visualized concentration of the labeled protein within the resin; (b) The simulated protein concentration distribution profiles within the resin.

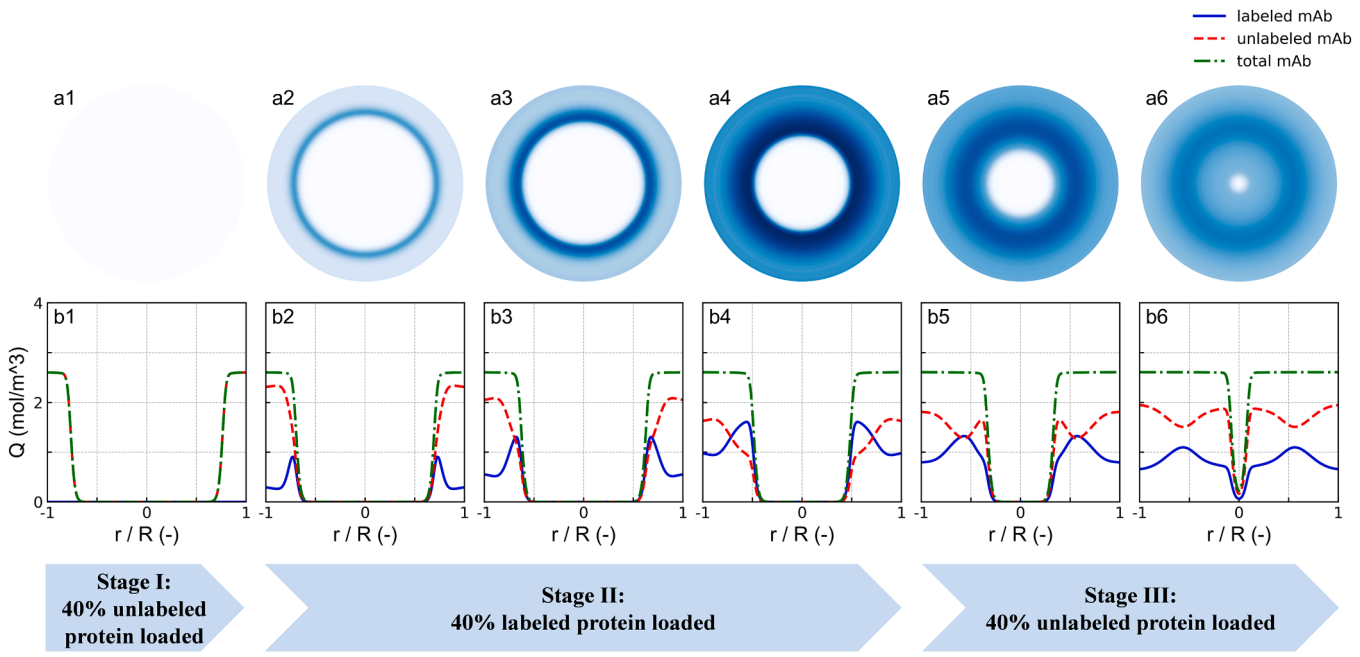

Fig. 9. Simulation results of CLSM for mAb during three load stages. (a)The visualized concentration of the labeled protein; (b) The simulated protein concentration distribution profiles within the resin.

resin penetration, mAb exhibited less leakage during the load and wash steps, as reflected in its lower ReTD profile compared to FC-protein (Figs. 6 and 7).

In summary, the mechanism of the exchange phenomenon within the resin was analyzed by the developed ReTD model. The model could accurately describe the CLSM images reported in the literature, particularly the liquid-solid exchange on the surface, providing a more comprehensive understanding of the ReTD behavior in Protein A chromatography process.

4.5. Impact of exchange effect on ReTD for continuous capture process

For continuous capture process, the interconnected load step complicates the material tracking. To investigate the impact of the exchange effect on ReTD in continuous capture, the interconnected load steps were simulated. Specifically, the protein was loaded into two interconnected columns until the second column reached 1 % breakthrough. The loaded protein was divided into two fractions: early-loaded and late-loaded proteins. Fig. 10 shows protein concentration profiles of the solid phase along the first and second columns at the end of interconnected load step. The results indicated that more protein loaded earlier was adsorbed into the second column when exchange effect was considered, compared to when it was neglected. During continuous capture, the resin is nearly fully loaded and the desorbed protein would move to the next column. Consequently, exchange effect might broaden the ReTD in continuous chromatography. Future studies will focus on ReTD modelling for the continuous capture process and further investigate the impact of the exchange effect on the material tracking for continuous process.

5. Conclusions

In this work, an ReTD model for Protein A affinity chromatography under high breakthrough conditions was developed, based on GRM and two-component mobile phase modulator Langmuir model. The model accounts both mass transfer and exchange effects. It was calibrated by static binding experiments and protein breakthrough curves with mAb and FC-fusion protein, achieving a high R^2 of 0.982 and 0.989. The pulse injection experiments with the labeled protein as the tracer under varying breakthrough percentage were used to validate the model prediction, which showed a good agreement with $R^2 > 0.945$. The results demonstrated that the ReTD model developed is effective for characterizing the ReTD behaviors in Protein A chromatography. Moreover, the model successfully described the CLSM images from the previous studies, explaining the liquid-solid exchange effect on the surface of resin and providing a more comprehensive understanding of the ReTD behavior in Protein A chromatography process. Finally, the model was used to simulate the protein distribution in the column during interconnected load step in continuous capture, highlighting that the exchange effect might broaden the ReTD in continuous chromatography. To our knowledge, it is the first time for the mechanistical modeling on ReTD behavior under high breakthrough conditions for Protein A chromatography process. Unlike conventional RTD models employed in other bioprocessing applications, such as the plug flow reactor (PFR) / continuous stirred tank reactor (CSTR) models for continuous viral inactivation or the tank-in-series (TIS) models for continuous virus filtration, the ReTD model developed in the present work incorporates the adsorption-desorption kinetics, which enables tracking the material within adsorption units. The results demonstrated that treating the tracer and normal protein as two components with identical mass transfer and adsorption-desorption kinetics in the chromatographic model is a feasible approach for ReTD modeling. However, there are some limitations in this work. This work focused specifically on the mass transfer dynamics during the interconnected loading step, rather than the entire continuous capture process. Future work will further develop the ReTD modeling for the whole continuous capture process and exploring its application in material tracking for continuous manufacturing. In general, production disturbances may occur at any stage of the process with various intensity and duration, potentially resulting in a non-confirming end product. The developed ReTD model can predict the propagation of non-conforming material, thereby enabling real-time decisions on diversion strategy for the continuous capture process to ensure consistent product quality.

CRediT authorship contribution statement

Wu-Wei Chen: Writing – original draft, Validation, Software, Methodology. **Yan-Na Sun:** Writing – review & editing. **Yu-Cheng**

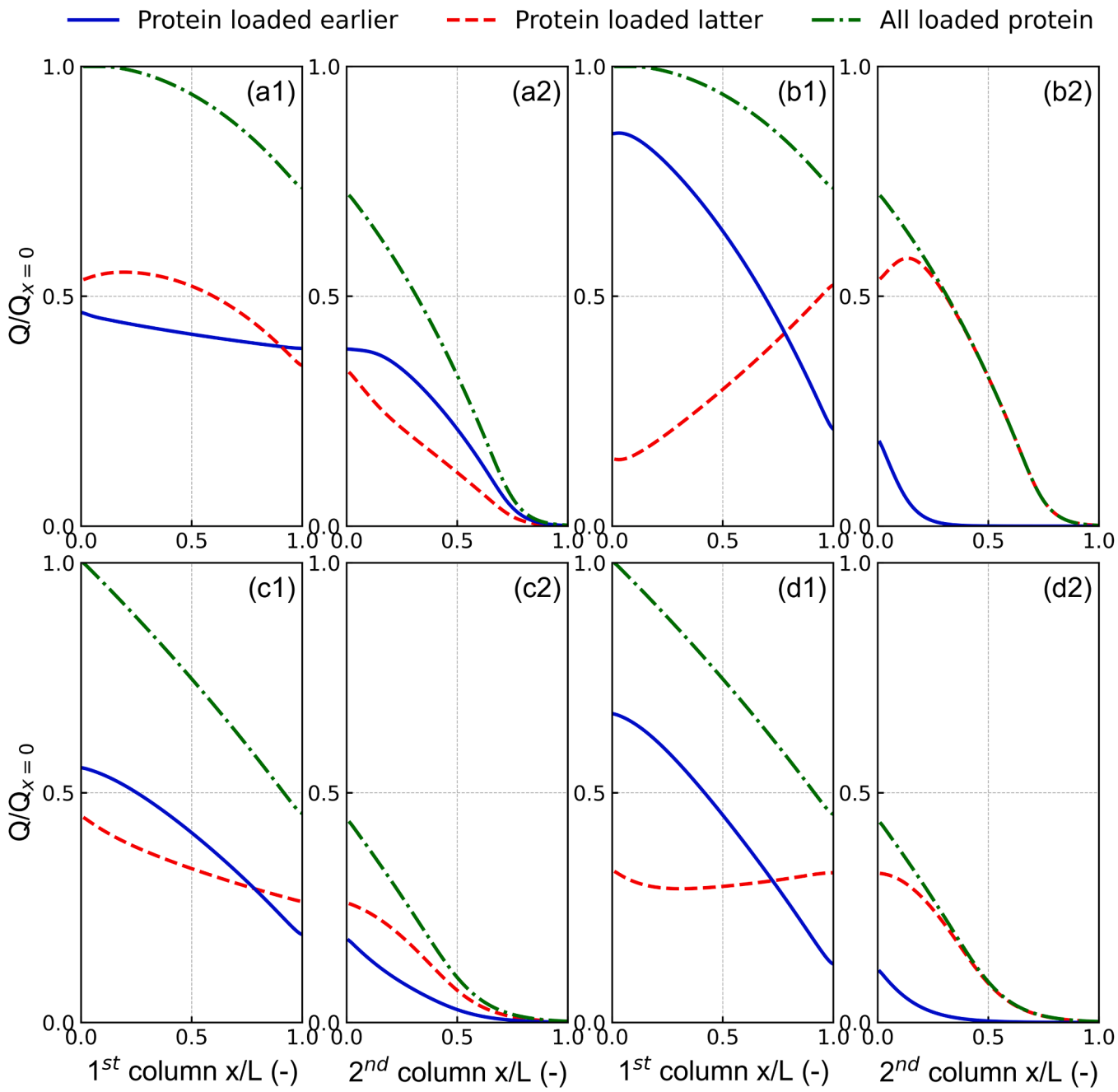

Fig. 10. Protein concentration profiles of solid phase along the first and second columns at the end of interconnected load step. (a) mAb with exchange effect; (b) mAb without exchange effect; (c) FC-protein with exchange effect; (d) FC-protein without exchange effect.

Chen: Writing – review & editing. **Alois Jungbauer:** Writing – review & editing. **Shan-Jing Yao:** Writing – review & editing. **Hai-Bin Qu:** Writing – review & editing. **Dong-Qiang Lin:** Writing – review & editing, Supervision, Funding acquisition, Conceptualization.

Declaration of competing interest

The authors declare that they have no known competing financial interests or personal relationships that could have appeared to influence the work reported in this paper.

Acknowledgements

This work was supported by the Zhejiang Key Science and Technology Project (2023C03116), National Natural Science Foundation of China (22078286) and National Key R&D Program of China (2021YFE0113300).

Supplementary materials

Supplementary material associated with this article can be found, in the online version, at doi:10.1016/j.chroma.2025.466227.

Data availability

Data will be made available on request.

References

[1] A. Jungbauer, Continuous downstream processing of biopharmaceuticals, Trends Biotechnol. 31 (2013) 479–492, https://doi.org/10.1016/j.tibtech.2013.05.011.

[2] A.S. Rathore, G. Thakur, N. Kateja, Continuous integrated manufacturing for biopharmaceuticals: a new paradigm or an empty promise? Biotechnol. Bioeng. 120 (2023) 333–351, https://doi.org/10.1002/bit.28235.

[3] L. David, P. Schwan, M. Lobedann, S.O. Borchert, B. Budde, M. Temming, M. Kuerschner, F.M. Alberti Aguilo, K. Baumarth, T. Thüte, B. Maiser, A. Blank, V. Kistler, N. Weber, H. Brandt, M. Poggel, K. Kaiser, K. Geisen, F. Oehme, G. Schembecker, Side-by-side comparability of batch and continuous downstream for the production of monoclonal antibodies, Biotechnol. Bioeng. 117 (2020) 1024–1036, https://doi.org/10.1002/bit.27267.

[4] O. Khanal, A.M. Lenhoff, Developments and opportunities in continuous biopharmaceutical manufacturing, MAbs. 13 (2021) 1903664, https://doi.org/10.1080/19420862.2021.1903664.

[5] C. Shi, X.J. Chen, B. Jiao, P. Liu, S.Y. Jing, X.Z. Zhong, R. Chen, W. Gong, D.Q. Lin, Model-assisted process design for better evaluation and scaling up of continuous downstream bioprocessing, J. Chromatogr. A 1683 (2022) 463532, https://doi.org/10.1016/j.chroma.2022.463532.

[6] A.S. Rathore, A. Bhargava, Biosimilars in developed economies: overview, status, and regulatory considerations, Regul. Toxicol. Pharm. 110 (2020) 104525, https://doi.org/10.1016/j.yrtph.2019.104525.

[7] Continuous manufacturing of drug substances and drug products Q13. https://database.ich.org/sites/default/files/ICH_Q13_Step4_Guideline_2022_1116.pdf.

[8] A.C. Fisher, M.H. Kamga, C. Agarabi, K. Brorson, S.L. Lee, S. Yoon, The current scientific and regulatory landscape in advancing integrated continuous biopharmaceutical manufacturing, Trends Biotechnol. 37 (2019) 253–267, https://doi.org/10.1016/j.tibtech.2018.08.008.

[9] N Lali, A Jungbauer, P Satzer, Traceability of products and guide for batch definition in integrated continuous biomanufacturing, J. Chem. Technol. Biotechnol. 97 (2022) 2386–2392, https://doi.org/10.1002/jctb.6953.

[10] A.E. Rodrigues, Residence time distribution (RTD) revisited, Chem. Eng. Sci. 230 (2021) 116188, https://doi.org/10.1016/j.ces.2020.116188.

[11] J. Sencar, N. Hammerschmidt, A. Jungbauer, Modeling the residence time distribution of integrated continuous bioprocesses, Biotechnol. J. 15 (2020) e2000008, https://doi.org/10.1002/biot.202000008.

[12] M.R. Brown, R. Orozco, Utilizing bacteriophage to define the minimum residence time within a plug flow reactor, Biotechnol. Bioeng. 118 (2021) 3367–3374, https://doi.org/10.1002/bit.27734.

[13] L. Amarikwa, R. Orozco, M. Brown, J. Coffman, Impact of Dean vortices on the integrity testing of a continuous viral inactivation reactor, Biotechnol. J. 14 (2019) e1700726, https://doi.org/10.1002/biot.201700726.

[14] M.S. Hong, A.E. Lu, R.W. Ou, J.M. Wolfrum, S.L. Springs, A.J. Sinskey, R.D. Braatz, Model-based control for column-based continuous viral inactivation of biopharmaceuticals, Biotechnol. Bioeng. 118 (2021) 3215–3224, https://doi.org/10.1002/bit.27846.

[15] Y.C. Chen, G. Recanati, F. De Mathia, D.Q. Lin, A. Jungbauer, Residence time distribution in continuous virus filtration, Biotechnol. Bioeng. 121 (2024) 1876–1888, https://doi.org/10.1002/bit.28696.

[16] A. Malakian, S.Y. Jung, M.A. Afzal, C. Carbrello, S. Giglia, M. Johnson, C. Miller, W. Rayfield, D. Boenitz, D. Cetlin, A.L. Zydney, Development of a transient inline spiking system for evaluating virus clearance in continuous bioprocessing-proof of concept for virus filtration, Biotechnol. Bioeng. 119 (2022) 2134–2141, https://doi.org/10.1002/bit.28119.

[17] G. Recanati, N. Lali, F. De Mathia, A. Jungbauer, Residence time distribution of continuous capture of recombinant antibody by precipitation and two stage tangential flow filtration, J. Chem. Technol. Biotechnol. 99 (2024) 1201–1211, https://doi.org/10.1002/jctb.7623.

[18] G. Recanati, M. Pappenreiter, C. Gstoettner, P. Scheidl, E.D. Vega, B. Sissolak, A. Jungbauer, Integration of a perfusion reactor and continuous precipitation in an entirely membrane-based process for antibody capture, Eng. Life Sci. 23 (2023) e2300219, https://doi.org/10.1002/elsc.202300219.

[19] T. Brantley, J. Bogue, K. Denny, S. Elouafiq, S. Madren, B. Nakhle, S. Khattak, A novel approach to residence time distribution characterization in a mAb continuous process, Biotechnol. Bioeng. 118 (2021) 3486–3498, https://doi.org/10.1002/bit.27775.

[20] N. Lali, P. Satzer, A. Jungbauer, Residence time distribution in counter-current protein A affinity chromatography using an inert tracer, J. Chromatogr. A 1683 (2022) 463530, https://doi.org/10.1016/j.chroma.2022.463530.

[21] C. Shi, Q.L. Zhang, B. Jiao, X.J. Chen, R. Chen, W. Gong, S.J. Yao, D.Q. Lin, Process development and optimization of continuous capture with three-column periodic counter-current chromatography, Biotechnol. Bioeng. 118 (2021) 3313–3322, https://doi.org/10.1002/bit.27689.

[22] C. Shi, Z.Y. Gao, Q.L. Zhang, S.J. Yao, N.K.H. Slater, D.Q. Lin, Model-based process development of continuous chromatography for antibody capture: a case study with twin-column system, J. Chromatogr. A 1619 (2020) 460936, https://doi.org/10.1016/j.chroma.2020.460936.

[23] Y.N. Sun, C. Shi, Q.L. Zhang, S.J. Yao, N.K.H. Slater, D.Q. Lin, Model-based process development and evaluation of twin-column continuous capture processes with protein A affinity resin, J. Chromatogr. A 1625 (2020) 461300, https://doi.org/10.1016/j.chroma.2020.461300.

[24] B. Somasundaram, K. Pleitt, E. Shave, K. Baker, L.H.L. Lua, Progression of continuous downstream processing of monoclonal antibodies: current trends and challenges, Biotechnol. Bioeng. 115 (2018) 2893–2907, https://doi.org/10.1002/bit.26812.

[25] D.Q. Lin, Q.L. Zhang, S.J. Yao, Model-assisted approaches for continuous chromatography: current situation and challenges, J. Chromatogr. A 1637 (2021) 461855, https://doi.org/10.1016/j.chroma.2020.461855.

[26] M. Angarita, T. Müller-Späth, D. Baur, R. Lievrouw, G. Lissens, M. Morbidelli, Twin-column CaptureSMB: a novel cyclic process for protein A affinity chromatography, J. Chromatogr. A 1389 (2015) 85–95, https://doi.org/10.1016/j.chroma.2015.02.046.

[27] J. Pollock, G. Bolton, J. Coffman, S.V. Ho, D.G. Bracewell, S.S. Farid, Optimising the design and operation of semi-continuous affinity chromatography for clinical and commercial manufacture, J. Chromatogr. A 1284 (2013) 17–27, https://doi.org/10.1016/j.chroma.2013.01.082.

[28] X. Gjoka, K. Rogler, R.A. Martino, R. Gantier, M. Schofield, A straightforward methodology for designing continuous monoclonal antibody capture multi-column chromatography processes, J. Chromatogr. A 1416 (2015) 38–46, https://doi.org/10.1016/j.chroma.2015.09.005.

[29] N.J. Hilbold, X.L. Saoût, E. Valery, L. Muhr, J. Souquet, A. Lamproye, H. Broly, Evaluation of several protein a resins for application to multicolumn chromatography for the rapid purification of fed-batch bioreactors, Biotechnol. Prog. 33 (2017) 941–953, https://doi.org/10.1002/btpr.2465.

[30] E.V. Lieres, J. Andersson, A fast and accurate solver for the general rate model of column liquid chromatography, Comput. Chem. Eng. 34 (2010) 1180–1191, https://doi.org/10.1016/j.compchemeng.2010.03.008.

[31] H.S. Traub, M. Schulte, A.S. Morgenstern, Preparative Chromatography, 3rd ed., Wiley, Germany, 2020. Available: https://onlinelibrary.wiley.com/doi/book/10.1002/9783527816347.

[32] S. Golshanshirazi, G. Guiochon, Modeling of preparative liquid-chromatography, J. Chromatogr. A 658 (1994) 149–171, https://doi.org/10.1016/0021-9673(94)80013-8.

[33] W. Heymann, J. Glaser, F. Schlegel, W. Johnson, P. Rolandi, E. von Lieres, Advanced score system and automated search strategies for parameter estimation in mechanistic chromatography modeling, J. Chromatogr. A 1661 (2022) 462693, https://doi.org/10.1016/j.chroma.2021.462693.

[34] S. Chan, N. Titchener-Hooker, D.G. Bracewell, E. Sørensen, A systematic approach for modeling chromatographic processes— Application to protein purification, AIChE J. 54 (2008) 965–977, https://doi.org/10.1002/aic.11441.

[35] E.J. Wilson, C.J. Geankoplis, Liquid mass transfer at very low reynolds numbers in packed beds, Ind. Eng. Chem. Fundam. 5 (1966) 9–14, https://doi.org/10.1021/i160017a002.

[36] T.M. Pabst, J. Thai, A.K. Hunter, Evaluation of recent protein A stationary phase innovations for capture of biotherapeutics, J. Chromatogr. A 1554 (2018) 45–60, https://doi.org/10.1016/j.chroma.2018.03.060.

[37] J. Guo, S. Noyes, W. Jin, H. Curtis, X. Xu, S. Ghose, Effect of solution condition on the binding behaviors of monoclonal antibody and fusion protein therapeutics in Protein A chromatography, J. Chromatogr. A 1686 (2022) 463652, https://doi.org/10.1016/j.chroma.2022.463652.

[38] O. Levenspiel, Chemical Reaction Engineering, 3rd ed., Wiley, New York, 1999. Available: http://app.knovel.com/web/toc.v/cid:kpCREE0005.

[39] M. Zhu, G. Carta, Protein adsorption equilibrium and kinetics in multimodal cation exchange resins, Adsorption 22 (2016) 165–179, https://doi.org/10.1007/s10450-015-9735-z.

[40] D. Karlsson, N. Jakobsson, A. Axelsson, B. Nilsson, Model-based optimization of a preparative ion-exchange step for antibody purification, J. Chromatogr. A 1055 (2004) 29–39, https://doi.org/10.1016/j.chroma.2004.08.151.